Transport and Communications Science Journal

DETECTION OF BEARING FAULTS BASED ON BAND-PASS FILTERS AND FOURIER INTERPOLATION OF THE LOAD TORQUE

Van Trang Phung[1], Thanh Lich Nguyen[2*]

[1]Viettel High Technology Industries Corporation, No 380 Lac Long Quan Street, Hanoi, Vietnam

[2]University of Transport and Communications, No 3 Cau Giay Street, Hanoi, Vietnam

ARTICLE INFO

TYPE: Research Article
Received: 14/07/2023
Revised: 21/08/2023
Accepted: 23/08/2023
Published online: 15/09/2023
https://doi.org/10.47869/tcsj.74.7.2

* *Corresponding author*
Email: lichnt@utc.edu.vn

Abstract. Bearing faults are widely found in mechatronics systems especially those that are required to work with unbalance loads. A highly reliable mechatronics system requires high quality bearings and/or effective bearing fault diagnostic procedure. This paper deals with the detection of rolling bearing faults based on band-pass filters and Fourier interpolation of the load torque. The reference torque, which is the output of the speed controller, is considered to be an approximation of the load torque. The reference torque is band-pass filtered and then interpolated in terms of Fourier series by using a sliding window method. The Fourier coefficients associated with a healthy bearing are served as a baseline and are compared with faulty lines corresponding to faulty bearings to detect the presence of a bearing failure. The proposed diagnostic method can be conducted online and does not require any additional sensors. Furthermore, the proposed method is able to detect single-point defects whose faulty levels are located at level C of the ISO 10816 Part 3. A mechatronic system equipped with artificial bearing faults is built in the laboratory to verify the effectiveness of the proposed method.

Keywords: Bearing faults, band-pass filter, Fourier interpolation.

1. INTRODUCTION

Mechatronics systems characterized by electrical and mechanical parts are commonly found in production processes. The demand for a highly reliable and productive mechatronics system requires both the mechanical and electrical parts to be trustworthy. Among vital causes of mechanical and electrical malfunctions, bearing faults account for up to 40% of all failures [1]. The diagnosis of incipient bearing faults is therefore crucial in terms of improving the system's productivity and robustness.

There are numerous methods available in the literature dedicated to the detection of bearing faults. These methods can be divided into three main streams: model-based, signal-based and data-driven-based methods [2]. The first group is based on the detection of changes in the system's parameters caused by the bearing faults [3-4]. The model-based methods do not require additional sensors than those that were already installed in the industrial settings but it demands a deep understanding of the system, from which the mathematical model of the system can be constructed.

The signal-based methods tell whether or not a bearing fault occurs by analyzing measured signals that contain intrinsic information related to the faults [5-7]. The signal-based diagnostic methods are able to detect both single point defects in the inner raceway, outer raceway, as well as balls or cage of rolling bearings and can be conducted online or offline with/without the use of additional sensors.

Recently, data-driven-based methods have been investigated extensively and have gained considerable achievement [8-10]. It was proven that the multi-layer structure included in the deep learning framework can extract hidden discriminative features in the raw signals, then construct the relationship between the extracted features and the fault labels. However, it is difficult to implement the data-driven-based methods online due to the calculation burden required by the algorithm as the methods require additional sensors for obtaining a big amount of data.

In the field of diagnosis of rolling bearing faults, a simple method that can be implemented online without the use of additional sensors is still challenging. This paper proposes such a procedure that is based on band-pass filters and the Fourier interpolation of the load torque. The novelty of the proposed method lies in the analysis of the load torque augmented with band-pass filters and the sliding window method that allows the diagnostic algorithm to be conducted continuously during the operation of industrial settings. The proposed diagnostic algorithm can detect single-point defects on either the outer raceway or the inner raceway without the use of additional sensors. Artificial faulty bearings will be used to verify the effectiveness of the method.

It is necessary to mention that the adaptation of band-pass filters to detect characteristic or resonant frequencies caused by bearing faults has been developed by some research groups [11-13], who share the same idea of using vibration signals for their proposed diagnostic methods. The acquisition of vibration signals requires vibration or acceleration sensors that demands more investment and requires expertise for the operation of the sensors. In contrast, the diagnostic method presented in this work uses the reference torque, that is the output of the speed controller, to detect characteristic fault frequencies of the bearing faults. This means that our method does not require any additional sensors other than those that were already installed in the electrical drives.

Hereafter, the structure of the paper is organized as follows: characteristic fault frequencies of rolling bearings will be presented in Section 2 while Section 3 dedicates to the proposed diagnostic method. Section 4 focuses on the experiment results.

2. CHARACTERISTIC FAULT FREQUENCIES OF ROLLING BEARINGS

Figure 1 depicts the structure of a rolling bearing that consists of four main components, namely an outer raceway, a cage, balls, and an inner raceway. The load angle α is defined as the angle between the centerline of the bearing and the direction of the force that the rolling elements exert on the outer raceway [14]; $d_\mathrm{b}, d_\mathrm{c}, d_\mathrm{i}, d_\mathrm{o}$ are the diameter of the balls, the cage, the inner raceway and the outer raceway, respectively.

The outer raceway is often fixed inside the bearing housing. The characteristic fault frequencies of the four main single-point defects on the outer raceway f_ORF, on the inner raceway f_IRF, on the balls f_BF and on the cage f_CF are given as follows [15]:

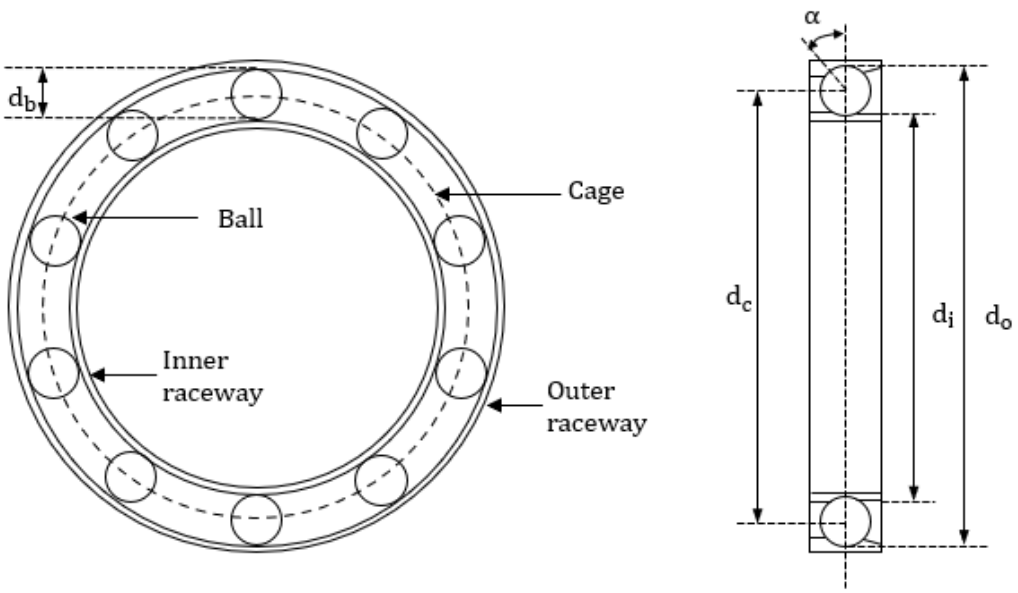

Figure 1. Graphical representation of a rolling bearing: the axial view (left) and the cross-section view (right).

$$f_\mathrm{ORF} = \frac{z}{2} \cdot f_\mathrm{n} \cdot \left(1 - \frac{d_\mathrm{b}}{d_\mathrm{c}} \cdot \cos\alpha\right) \tag{1}$$

$$f_\mathrm{IRF} = \frac{z}{2} \cdot f_\mathrm{n} \cdot \left(1 + \frac{d_\mathrm{b}}{d_\mathrm{c}} \cdot \cos\alpha\right) \tag{2}$$

$$f_\mathrm{BF} = \frac{d_\mathrm{c}}{2d_\mathrm{b}} \cdot f_\mathrm{n} \cdot \left(1 - \frac{d_\mathrm{b}^2}{d_\mathrm{c}^2} \cdot \cos^2\alpha\right) \tag{3}$$

$$f_{\mathrm{CF}} = \frac{1}{2} \cdot f_{\mathrm{n}} \cdot \left(1 - \frac{d_{\mathrm{b}}}{d_{\mathrm{c}}} \cdot \cos\alpha\right) \quad (4)$$

where z is the number of bearing balls and f_{n} is the rotational frequency of the inner raceway. It can be seen from (1)-(4) that the characteristic fault frequencies depend on the mechanical dimension and velocity of the undertested bearing.

When a bearing installed in an electrical machine degrades and enters faulty condition, it can create changes in the load torque whenever the bearing balls go over the damaged areas. This natural phenomenon results in characteristic fault frequencies hidden in the spectrum of the load torque. The idea behind the method proposed in this paper regarding the detection of such characteristic fault frequencies that will be elaborated in Section 3.

As inner and outer raceway faults are found up to 90% of all bearing failures [16], this research work will focus mainly on these two types of bearing faults. For bearings with six to twelve bearing balls, the outer and inner characteristic fault frequencies given in (1) and (2) can be approximated as follows [17]:

$$f_{\mathrm{ORF}} = 0.4 \cdot z \cdot f_{\mathrm{n}} \quad (5)$$

$$f_{\mathrm{IRF}} = 0.6 \cdot z \cdot f_{\mathrm{n}} \quad (6)$$

3. PROPOSED METHOD FOR THE DETECITON OF BEARING FAULTS

As the load torque contains intrinsic information related to the bearing faults, it can be used in a diagnostic algorithm whose outputs provide information about whether or not the undertested bearing is suffering from any kinds of damages. The load torque can be measured by using load sensors but this approach leads to additional cost. A promising solution to estimate the load torque is the use of a state observer or Kalman filter [18-19] that was proven successful to be conducted online with high precision. In this paper, a very simple way for obtaining the information of the load torque is based on an assumption that if the speed controller is properly designed, the reference torque which is the output of the speed controller can be regarded as a good approximation of the load torque. The reference torque will be used in the diagnostic algorithm.

3.1. Proposed diagnostic method

As mentioned in Section 2, the spectrum of the load torque contains hidden information related to the characteristic fault frequencies. Obviously, the load torque consists of other harmonics than those related to the bearing faults. So, there is a rising question on how to extract the hidden information of characteristic fault frequencies in the spectrum of the load torque. By utilizing the load torque to detect bearing faults, the proposed diagnostic algorithm does not require any additional sensors. This is one of the novelties of our proposed method.

Figure 2 shows the schematic of the proposed diagnostic procedure that is composed of three main components: the band-pass filter (BPF), the fast Fourier transformation (FFT) and the fault decision-making (FDM). ω^* and ω are the reference and measured velocities, respectively. C_ω is the velocity controller where a proportional-integral (PI) structure designed upon the symmetrical optimum criteria is often adopted.

The BPF is designed so that its specific frequencies are the characteristic fault frequencies of the bearing faults. In this way, the BPF is able to remove frequencies unrelated to the faults. The Fast Fourier Transform (FFT) augmented with a sliding window method is used to calculate the magnitude of each harmonic component of the Fourier expansion of the filtered load torque. Since the sliding window can be conducted online, the diagnostic algorithm can be implemented continuously during the operation of the mechatronic systems. This is the other novelty of this research work. The harmonics' coefficients associated with a healthy bearing are used as a base line and are compared with faulty lines corresponding to faulty bearings. The fault decision-making uses the differences between the two lines to decide the type of bearing faults. The working principle of the BPF and FFTs is presented below.

3.2. Band-pass filter (BPF)

As aforementioned, the BPF is composed of multiple band-pass filters where each of them is designed with a specific frequency defined by the characteristic fault frequencies. The transfer function of the BPF is given by:

$$\mathrm{BPF}(s) = \sum_{\omega_\mathrm{i}} \frac{\frac{\omega_\mathrm{i}}{Q_\mathrm{i}} \cdot s}{s^2 + \frac{\omega_\mathrm{i}}{Q_\mathrm{i}} \cdot s + \omega_\mathrm{i}^2} \tag{7}$$

where $\omega_\mathrm{i} = 2\pi \cdot f_\mathrm{i}$ with f_i is the considered frequency; Q_i is the quality factor. The considered frequency f_i can be adaptively selected according to (5) and (6) which depends on the operating velocity of the undertested bearing. The quality factor affects the filtering behavior of the band-pass filter. The increase of Q_i results in a stronger band-pass filter in terms of disturbance rejection.

Another concern associated with the implementation of the BPF is the discretization method that has to ensure a precise amplitude and/or root locus responses. There are different ways for discretizing the BPF, such as zero-order hold (ZOH), triangle approximation (First-order hold - FOH), impulse invariant (impulse), Tustin, zero-pole matching (matched) and least-square method (least-square) [20].

The discretization methods do not exhibit considerable differences around the characteristic frequency but strongly affect the magnitude response of the BPF when the ratio between the sampling frequency and the characteristic frequency of the BPF is insignificant ($f_\mathrm{i}/f_\mathrm{s} \ll 0.2$). Figure 3 depicts the Bode plot of a BPF according to different discretization methods where $f_\mathrm{s} = 5$ kHz, $f_\mathrm{i} = 1$ kHz, $Q_\mathrm{i} = 1$. The zoom-in portion of the magnitude response around $f_\mathrm{i} = 1$ kHz shows that the least-square method provides the most precise amplitude response around the characteristic frequency of the BPF. The other discretization methods signify or diminish the amplitude at f_I, hence they are unsuitable choices.

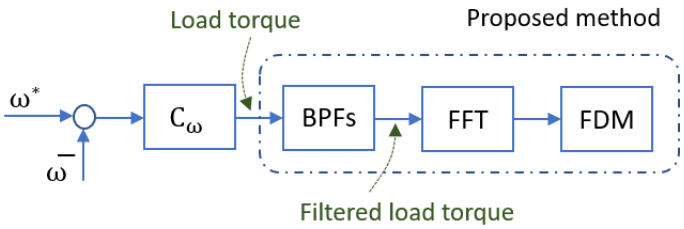

Figure 2. The schematic of the diagnostic procedure.

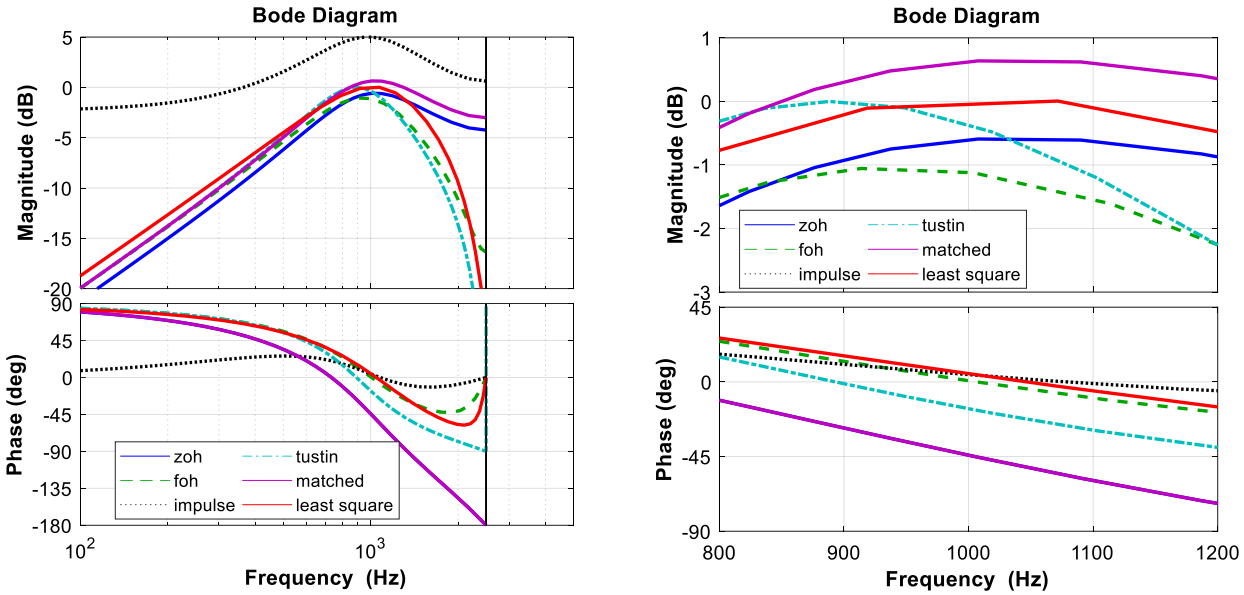

Figure 3. Bode plot of a band-pass filter according to different discretization methods (with sampling time $f_s = 5$ kHz, $f_i = 1$ kHz, $Q_i = 1.0$): (left) the original Bode plot; (right) the zoom-in portion at the characteristic frequency $f_i = 1$ kHz.

3.3. Fast Fourier Transformation (FFT)

As aforementioned the BPF aims to ignore unwanted harmonics in the measured signal. The output of the BPF is the filtered signal that now mainly contains harmonics related to faulty frequencies. The filtered signal is undergone a fast Fourier transform algorithm to extract desired information buried in its spectrum. For conducting the diagnostic algorithm online, a sliding-window method can be used for the FFT. The working principle of the sliding window method is as follows:

Supposing that the filtered signal is expanded in terms of Fourier series as a function of γ_m [21].

$$T_{\text{filter}} = a_0 + \sum_{k=1}^{\infty} \left(a_k \cdot \cos(k \cdot \gamma_m) + b_k \cdot \sin(k \cdot \gamma_m) \right) \tag{8}$$

where:

$$a_k = \frac{2}{N} \cdot \sum_{j=0}^{N-1} T_{\text{filter}}(j \cdot \Delta\gamma_m) \cdot \cos(k \cdot j \cdot \Delta\gamma_m);\ b_k = \frac{2}{N} \cdot \sum_{j=0}^{N-1} T_{\text{filter}}(j \cdot \Delta\gamma_m) \cdot \sin(k \cdot j \cdot \Delta\gamma_m);\ \Delta\gamma_m = \frac{2\pi}{N}$$

N is the number of samples per one period of T_{filter}. The function of the sliding-window method is to calculate Fourier coefficients a_k and b_k while γ_m changes with time (sliding). The figure representation of the sliding window method is shown in Figure 4. The sliding-window method has some highlighted properties as follows. First, the online implementation converges after exactly one period of the input signal. Second, the number of samples per signal period N should be chosen properly. The higher the value of N, the more precise estimation of the Fourier coefficients but the more calculation and storage required by the calculation of the sliding-window method. From extensive experiments, $N \geq 8$ ensures a good estimation precision when the method is implemented online and the bearing is operated at high speed.

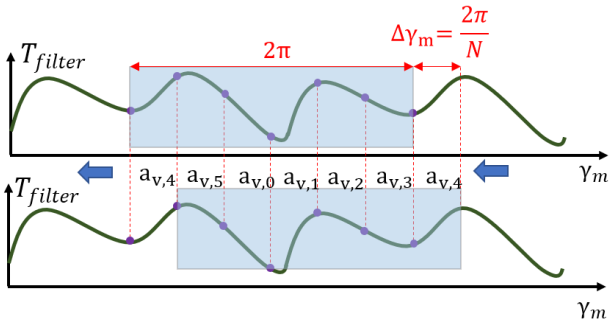

Figure 4. Figure representation of the sliding-window method.

3.4. Fault decision making (FDM)

According to the spectrum of the filtered load torque obtained from the BPF, the fault decision-making will decide whether or not the bearing is suffering from a defect. It is important to note that the detectable faulty level of the bearing is located at level C of the ISO 10816 standard part 3 [22], where the bearing still offers normal functionality but maintenance should be considered.

The FDM uses the spectrum of the filtered load torque with a healthy bearing as the baseline and is compared with faulty lines associated with faulty bearings. If there are significant differences in the outer raceway characteristic fault frequency and its multiples, the undertested bearing is diagnosed to have an outer raceway. The same situation is applied to the inner raceway failure. The working principle of the FDM will be presented in detail in the experimental result hereafter.

4. PROPOSED METHOD FOR THE DETECITON OF BEARING FAULTS

In this section, experiments will be presented to validate the effectiveness of the proposed method. The first section dedicates to the description of the testbench followed by the preparation of desired faulty bearings. Experiment results will be presented lastly to confirm the operation of the proposed diagnostic algorithm.

4.1. Description of the testbench

Figure 5 shows the mechatronic system used to verify the operation of the diagnostic method. The mechatronic system is a horizontal slider-crank mechanism that is characterized by repetitive load torque and commonly found in industrial settings, like pick and place machines, punching machines or robotic arms. There are two bearings in between the driving permanent magnet synchronous machine (PMSM) and the mechanical system: one is located in the load side and the other is installed in the machine side. The undertested faulty bearing is UC 205 whose graphical dimension is depicted in Figure 6. The testing bearing is placed on the load side. The parameters of the driving machine are given in Table 1 while that of the bearing are given in Table 2. The field-oriented control algorithm for the PMSM is conducted by a high performance dSPACE 1104 board.

4.2. Preparation of artificial faulty bearings

As already mentioned in Section 3, the diagnostic algorithm is developed to be able to detect bearing faults located at level C of the ISO 10816 Part 3 standard. It is therefore crucial to prepare artificial faulty bearings at desired faulty level. Figure 7 shows the levels of rolling bearing faults classified based on the vibration velocity measured at the housing of the bearings.

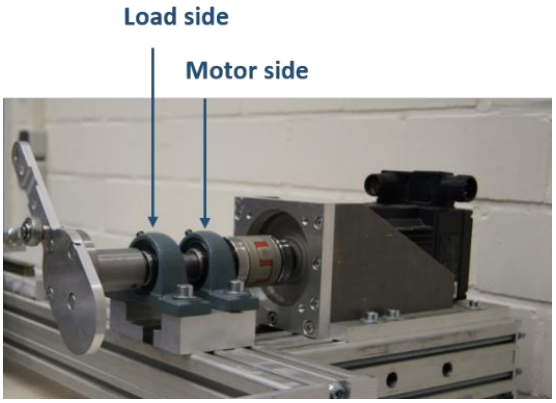

Figure 5. Experimental setup.

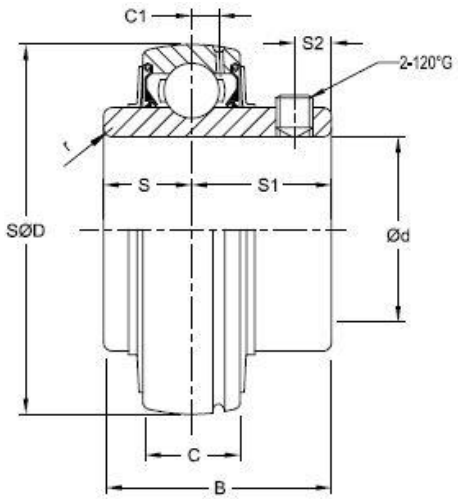

Figure 6. Graphical dimension of the testing bearing UC 205.

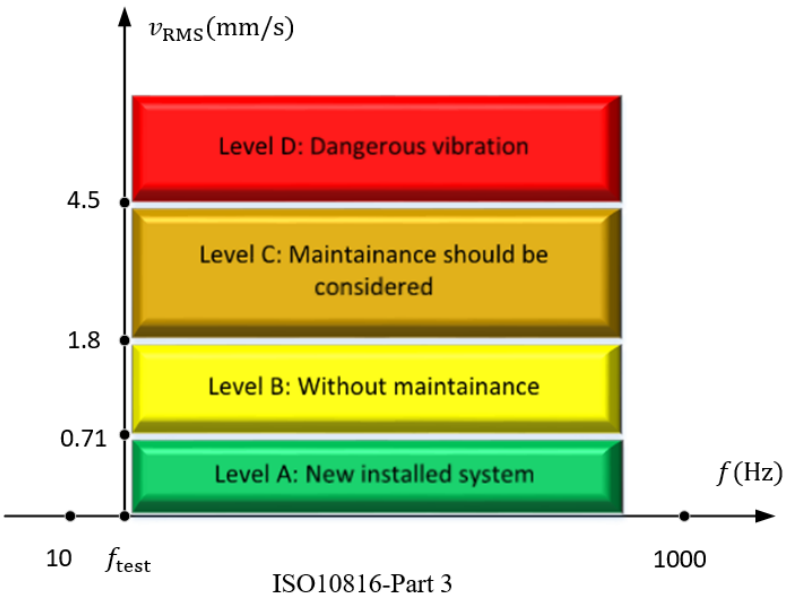

Figure 7. ISO 10816 Part 3 for classification of faulty levels of rolling bearing.

Figure 8 shows the case of an outer raceway defect, where a hole on the housing and a hole on the outer raceway were created that allow a screw to go up and down to change the pressure contact with the bearing balls. The location of the screw is set so that the vibration velocity measured at the housing of the bearing categorizes the faulty level of the undertested bearing at level C of the ISO 10816 standard. Figure 9 depicts the vibration velocity measured by an MMF KSI 80VB vibration sensor at the housing of the faulty bearing while the system was running at 1000 rpm. It is observed in Figure 9 that the vibration velocity measured with a healthy bearing (in the red) is small and is categorized at level B while the faulty bearing is at level C (the blue line).

Table 1. Parameters of the driving machine.

Parameters	**Value**	**Unit**
Machine model	ABB SDM 101-005N8-115	
Nominal power	1.54	kW
Nominal velocity	3000	rpm
Nominal torque	4.9	Nm
Number of pole pairs	3	
Moment of inertia	0.0006	$kg.m^2$

Table 2. Parameters of the testing bearings.

Parameters	**Value**	**Unit**
Load angle, α	0	degree
Outer diameter, D	52	mm
Inner diameter, d	25	mm
Inside ring width, B	34.1	mm
Outside ring width, C	17	mm
Radius, r	1	mm
Groove position, C1	4.0	mm
Dimension, S1	19.8	mm
Number of balls, z	9	balls

For preparing an inner raceway fault, a hole in the shaft and a hole in the inner raceway were created that allow the screw to go up and down inside the shaft and touch the ball bearings as shown in Figure 10. The location of the screw is changed until the vibration velocity measured on the bearing housing tells us that the faulty level is at level C of the ISO 10816 standard. The vibration velocity is depicted in Figure 11.

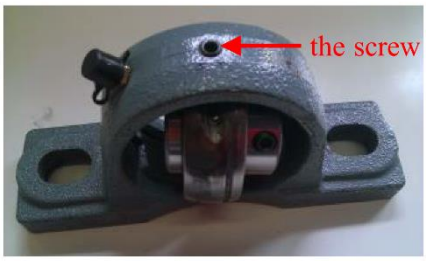

Figure 8. Bearing with artificial outer raceway defect.

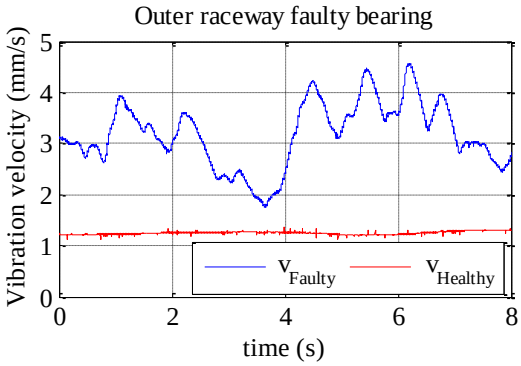

Figure 9. Vibration velocity corresponding to an artificial outer raceway fault.

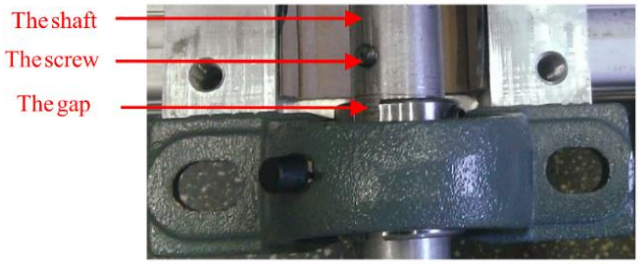

Figure 10. Bearing with an artificial inner raceway fault.

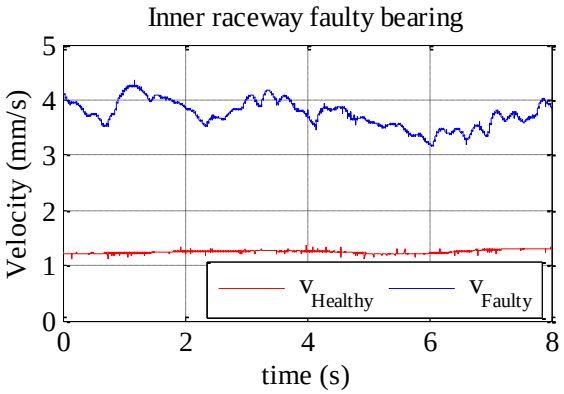

Figure 11. Vibration velocity corresponding to an artificial inner raceway fault.

4.3. Verification of the proposed diagnostic method

Experiments with the outer raceway defect are presented first. Figure 12 shows the reference torque that is the output of the conventional proportional-integral controller with a healthy bearing (lower figure) and with an outer raceway fault (upper figure). It is observed that the reference torque changes periodically according to the rotor angle as the mechatronic system is characterized by a repetitive load cycle. The system is driven at 60 rpm resulting $f_{\mathrm{n}} = 1$ Hz. The ten-seconds sample is undergone the diagnostic algorithm meaning that $f_{\mathrm{n}} = 10$ Hz and the outer characteristic fault frequency of the outer raceway defect given in (5) is:

$$f_{\mathrm{ORF}} = 0.4 \cdot z \cdot f_{\mathrm{n}} = 0.4 \cdot 9 \cdot 10 = 36 \text{ Hz} \tag{10}$$

The BPF is designed with $f_{\mathrm{i}} = i \cdot f_{\mathrm{ORF}}$ with $i = 1 \div 4$ and the quality factor $Q_{\mathrm{i}} = 0.7$. The least-square discretization method is adopted. The spectrum of the filtered load torque depicted in Figure 13 clearly shows considerable differences between the baseline obtained from a healthy bearing and the faulty line associated with the outer raceway defective bearing. The fault decision making (FDM) can conclude that the outer raceway fault at level C of the ISO 10816 was successfully detected.

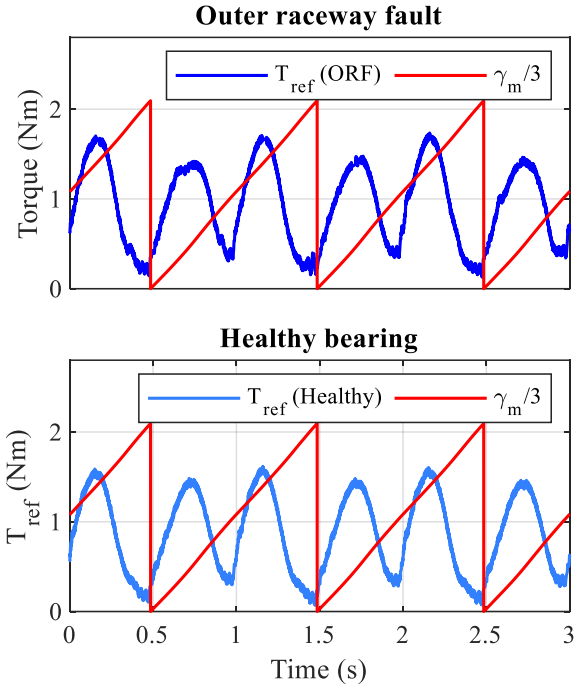

Figure 12. Reference torque and rotor mechanical angle: (upper) outer raceway fault; (lower) healthy bearing.

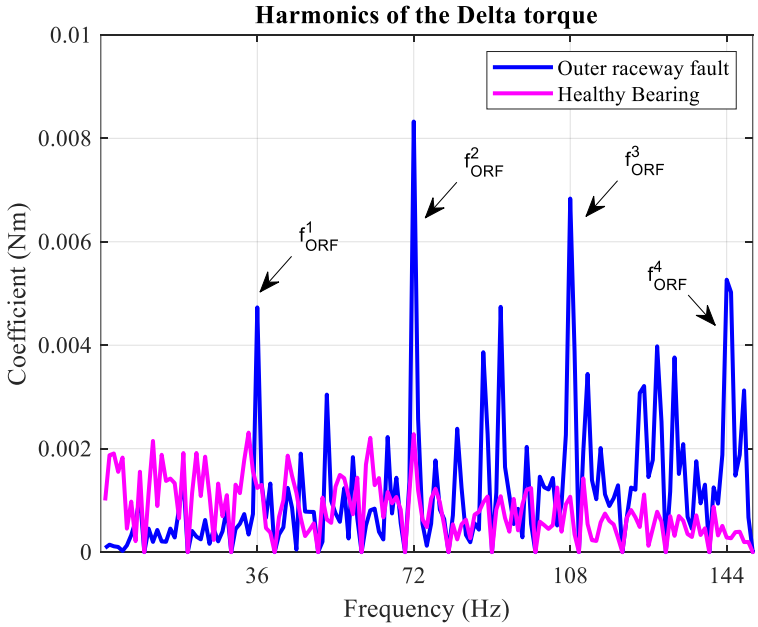

Figure 13. Spectrum of the load filtered load torque: harmonics up to the 4th of the f_{ORF} is considered; $Q_{\mathrm{i}} = 0.7$.

For the case of the inner raceway fault, the bearing with an artificial fault as prepared in Section 4 is tested. The reference torque and the rotor angle are depicted in Figure 14. It is proven again that the reference torque is a periodic function of the rotor angle. The characteristic fault frequency corresponding to the inner raceway fault defined by (6) is:

$$f_{\mathrm{IRF}} = 0.6 \cdot z \cdot f_{\mathrm{n}} = 0.6 \cdot 9 \cdot 10 = 54 \text{ Hz} \tag{11}$$

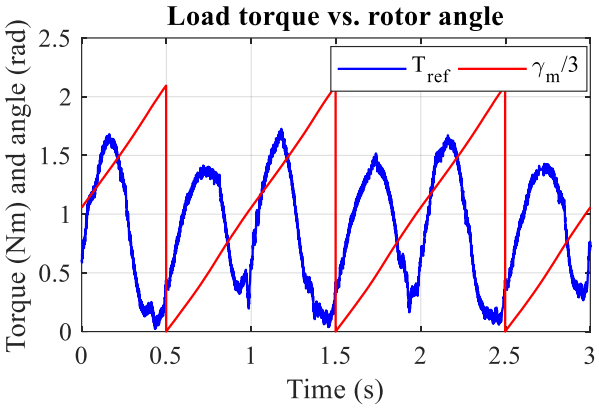

Figure 14. Reference torque and rotor mechanical angle: inner raceway fault.

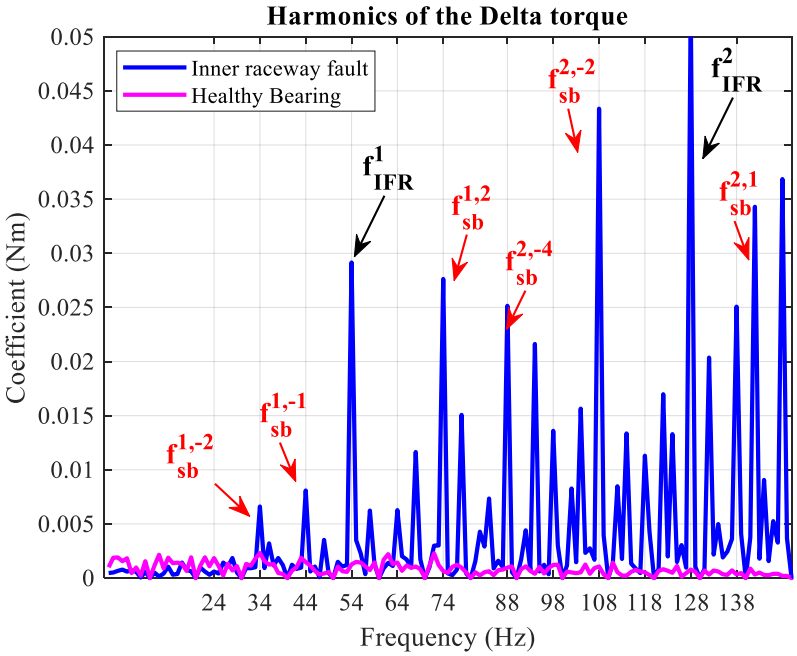

Figure 15. Spectrum of the load filtered load torque: harmonics up to the 2nd of the f_{IRF} is considered; $Q_i = 0.7$.

The spectrum of the filtered load torque is depicted in Figure 15 that shows significant differences between the faulty line and the baseline at f_{IRF} and its multiples. The inner raceway fault has a distinctive characteristic, namely the sideband effect. Besides the characteristic fault

frequency, the sideband frequencies defined (12) also serve as signatures for the detection of the inner raceway fault [23].

$$f_{\mathrm{sb}}^{i,k} = |i \cdot f_{\mathrm{IRF}} + k \cdot f_{\mathrm{n}}| \tag{12}$$

where i and k are integers. The sideband effect is caused by the unbalanced load zone distribution inside a bearing. It is well known that rolling elements in a bearing are not subjected to an equal load [24]. When the defect rotates through the load zone, an impulse will be created every time a ball passes over the damaged area. The intensity of the shock will be the greatest magnitude if the defect is located at the point of maximum radial torque. Therefore, the most intense impulse is generated on every turn of the machine, assuming that the inner raceway synchronously rotates with the shaft of the driven machine. This phenomenon leads to the fact that the intensity of the defect is modulated by the mechanical rotation frequency $\boldsymbol{f_{\mathrm{n}}}$. And interestingly the sideband effect is clearly observed in Figure 15, for examples: $f_{\mathrm{sb}}^{1,-2} = 34$ Hz, $f_{\mathrm{sb}}^{1,-1} = 44$ Hz, $f_{\mathrm{sb}}^{1,2} = 74$ Hz, $f_{\mathrm{sb}}^{2,-4} = 88$ Hz, $f_{\mathrm{sb}}^{2,-2} = 108$ Hz, $f_{\mathrm{sb}}^{2,1} = 138$ Hz . The FDM can conclude that the inner raceway fault at level C of the ISO 10816 standard was successfully detected.

5. CONCLUSIONS

In this paper, a novel algorithm based on band-pass filters and Fourier interpolation of the load torque for the detection of rolling bearing failure was proposed. The diagnostic algorithm was proven to successfully detect inner raceway and outer raceway defects at level C of the ISO 10816 Standard without the use of additional sensors rather than those that were already installed in a mechatronics system. The effectiveness of the proposed method was validated by experiments and can be conducted either online or offline during the operation of the mechatronics system.

ACKNOWLEDGMENT

This research is funded by University of Transport and Communications under grant number T2023-CK-001.

REFERENCES

[1]. W. F. Braun, B. G. Douglass, C. R. Heising, D. O. Koval, P. O'Donnell, EEE Recommended Practice for the Design of Reliable Industrial and Commercial Power Systems (Gold Book), IEEE Std 493-1997 IEEE Gold Book, (1998) 1–464. https://doi.org/10.1109/IEEESTD.1998.89291

[2]. X. Dai, Z. Gao, From Model, Signal to Knowledge: A Data-Driven Perspective of Fault Detection and Diagnosis, IEEE Trans. Ind. Inform., 9 (2013) 2226–2238. https://doi.org/10.1109/TII.2013.2243743

[3]. S. Zhang, Model-Based Analysis and Quantification of Bearing Faults in Induction Machines, IEEE Trans. Ind. Appl., 56 (2020) 2158–2170. https://doi.org/10.1109/TIA.2020.2979383

[4]. M. Ojaghi, M. Sabouri, J. Faiz, Analytic Model for Induction Motors Under Localized Bearing Faults, IEEE Trans. Energy Convers., 33 (2018) 617–626. https://doi.org/10.1109/TEC.2017.2758382

[5]. D. T. Hoang, H. J. Kang, A Motor Current Signal-Based Bearing Fault Diagnosis Using Deep Learning and Information Fusion, IEEE Trans. Instrum. Meas., 69 (2020) 3325–3333. https://doi.org/10.1109/TIM.2019.2933119

[6]. F. Dalvand, S. Dalvand, F. Sharafi, M. Pecht, Current Noise Cancellation for Bearing Fault Diagnosis Using Time Shifting, IEEE Trans. Ind. Electron., 64 (2017) 8138–8147. https://doi.org/10.1109/TIE.2017.2694397

[7]. E. Elbouchikhi, V. Choqueuse, F. Auger, M. E. H. Benbouzid, Motor Current Signal Analysis Based on a Matched Subspace Detector, IEEE Trans. Instrum. Meas., 66 (2017) 3260–3270. https://doi.org/10.1109/TIM.2017.2749858

[8]. L. Wen, X. Li, L. Gao, Y. Zhang, A New Convolutional Neural Network-Based Data-Driven Fault Diagnosis Method, IEEE Trans. Ind. Electron., 65 (2018) 5990–5998. https://doi.org/10.1109/TIE.2017.2774777

[9]. P. Cao, S. Zhang, J. Tang, Preprocessing-Free Gear Fault Diagnosis Using Small Datasets With Deep Convolutional Neural Network-Based Transfer Learning, IEEE Access, 6 (2018) 26241–26253. https://doi.org/10.1109/ACCESS.2018.2837621

[10]. T. Han, C. Liu, W. Yang, D. Jiang, Deep Transfer Network with Joint Distribution Adaptation: A New Intelligent Fault Diagnosis Framework for Industry Application, ISA Trans., 97 (2020) 269–281. https://doi.org/10.1016/j.isatra.2019.08.012

[11]. Y. Lu, Z. Song, Q. Gao, D. Zhu, D. Sun, Bearing fault diagnosis based on multi-band filtering, IET Sci. Meas. Technol., 16 (2022) 101–117. https://doi.org/10.1049/smt2.12090

[12]. W. Guo, An Optimal Band-pass Filter based on Adaptive Identification of Bearing Resonant Frequency Band, in 2020 Asia-Pacific International Symposium on Advanced Reliability and Maintenance Modeling (APARM), (2020) 1–7. https://doi.org/10.1109/APARM49247.2020.9209420

[13]. L. Wang, J. Xiang, A Simulation Based Band-Pass Filter to Improve the Polynomial Chirplet Transform in Fault Detection, in 2018 Prognostics and System Health Management Conference (PHM-Chongqing), (2018) 129–133. https://doi.org/10.1109/PHM-Chongqing.2018.00028

[14]. J. R. Stack, T. G. Habetler, R. G. Harley, Fault classification and fault signature production for rolling element bearings in electric machines, IEEE Trans. Ind. Appl., 40 (2004) 735–739. https://doi.org/10.1109/TIA.2004.827454

[15]. S. A. McInerny, Y. Dai, Basic vibration signal processing for bearing fault detection, IEEE Trans. Educ., 46 (2003) 149–156. https://doi.org/10.1109/TE.2002.808234

[16]. R. Rubini, U. Meneghetti, Application of the envelope and wavelet transform analyses for the diagnosis of incipient faults in ball bearings, Mech. Syst. Signal Process., 15 (2001) 287–302. https://doi.org/10.1006/mssp.2000.1330

[17]. M. E. H. Benbouzid, A review of induction motors signature analysis as a medium for faults detection, in Proceedings of the 24th Annual Conference of the IEEE Industrial Electronics Society, 4 (1998) 1950–1955. https://doi.org/10.1109/IECON.1998.724016

[18]. D. Pavkovic, J. Deur, I. Kolmanovsky, Adaptive Kalman Filter-Based Load Torque Compensator for Improved SI Engine Idle Speed Control, IEEE Trans. Control Syst. Technol., 17 (2009) 98–110. https://doi.org/10.1109/TCST.2008.922556

[19]. T. Shi, Z. Wang, C. Xia, Speed Measurement Error Suppression for PMSM Control System Using Self-Adaption Kalman Observer, IEEE Trans. Ind. Electron., 62 (2015) 2753–2763. https://doi.org/10.1109/TIE.2014.2364989

[20]. A. G. Yepes, F. D. Freijedo, J. Doval-Gandoy, Ó. López, J. Malvar, P. Fernandez-Comesaña, Effects of Discretization Methods on the Performance of Resonant Controllers, IEEE Trans. Power Electron., 25 (2010) 1692–1712. https://doi.org/10.1109/TPEL.2010.2041256

[21]. R. Isermann, Identifikation dynamischer Systeme: Band II: Parameterschätzmethoden, Kennwertermittlung und Modellabgleich, Zeitvariante, nichtlineare und Mehrgrößen-Systeme, Anwendungen. Berlin Heidelberg: Springer-Verlag, 1988. Accessed: (2021). [Online]. Available: https://www.springer.com/us/book/9783642970702

[22]. ISO Standard 10816, Mechanical Vibration-Elavuation of Machine Vibration by Measurement on Non-Rotating Parts- Part 3.
[23]. H. Zoubek, S. Villwock, M. Pacas, Frequency Response Analysis for Rolling-Bearing Damage Diagnosis, IEEE Trans. Ind. Electron., 55 (2008) 4270–4276. https://doi.org/10.1109/TIE.2008.2005020

[24]. J. R. Stack, T. G. Habetler, R. G. Harley, Fault-signature modeling and detection of inner-race bearing faults, IEEE Trans. Ind. Appl., 42 (2006) 61–68. https://doi.org/10.1109/TIA.2005.861365